Sensing and Bio-Sensing Research 46 (2024) 100686

Contents lists available at ScienceDirect

Sensing and Bio-Sensing Research

journal homepage: www.elsevier.com/locate/sbsr

A Fiber optics based surface enhanced Raman spectroscopy sensor for chemical and biological sensing

Jiayu Liu [a], Bohong Zhang [b], Amjed Abdullah [a], Sura A. Muhsin [a], Jie Huang [b], Mahmoud Almasri [a,*]

[a] Department of Electrical Engineering and Computer Science, University of Missouri, Columbia, MO 65211, USA
[b] Department of Electrical and Computer Engineering, Missouri University of Science and Technology, Rolla, MO 65409, USA

ARTICLE INFO

Keywords:
Microsphere photolithography
Side polished fiber
SERS
Fiber-optic Raman

ABSTRACT

This paper investigates an innovative surface-enhanced Raman scattering (SERS) sensor developed on a side-polished multimode optical fiber core. The optical fiber was integrated into specifically designed 3-dimensional printed mold, where manual polishing of the fiber took place. Microsphere Photolithography (MPL) techniques was employed to pattern periodic nanoantenna arrays on the polished surface, incorporating multiple disk diameters at a fixed periodicity. Subsequent gold deposition/lift-off were carried out to transfer the pattern from the photoresist to the fiber core, resulting in highly periodic hexagonal closed pack (HCP) arrays of nanodisks. These arrays can significantly enhance the SERS signal intensity compared to that of the fiber tip. The sensor's performance was demonstrated using various concentrations of Rhodamine 6G (R6G) dye ranging from 10^{-5} to 10^{-9} M as a function of disk diameter and sensing surface area. The resulting spectra revealed characteristic peak positions that aligned well with the fingerprint Raman spectra of R6G. The results demonstrates that the sensitivity is 10^{-9} M for the sensor with an 800 nm disk diameter.

1. Introduction

Raman spectroscopy, especially Surface Enhanced Raman spectroscopy (SERS), describes the interaction of light with the molecular composition and structure of a material, resulting in altered photon energy after scattering [1]. Molecules exhibit specific vibrational modes that generate distinct Raman spectral patterns. Due to the unique energy shifts of molecules, Raman spectroscopy enables qualitative and quantitative evaluation of chemical compositions. It serves as a powerful analytical tool with high detection sensitivity, molecular specificity, and the ability to probe solutions in the visible and near-infrared regions. Raman spectroscopy offers a plethora of label free and non-invasive diagnostic applications for molecular sensing including medical, environmental pollutants, pathogen, and nucleic acid targets sensing [2–8]. However, Raman scattering is inherently weak due to the low concentrations of molecules in the analyte, limiting the signal intensity of Raman spectra. To overcome this limitation and enhance the detection of low concentrations of analytes, SERS surfaces have been employed. These surfaces are intentionally roughened to amplify the Raman scattering signal by several orders of magnitude [9]. Surface Enhanced Raman Spectroscopy (SERS) indeed relies on the interaction between incident light and nanostructured metallic surfaces, typically composed of noble metals like gold or silver. These metallic nanostructures exhibit a phenomenon known as surface plasmon resonance (SPR), where free electrons oscillate collectively upon excitation by incident light at specific wavelengths. This resonance generates intense localized electromagnetic fields near the metal surface, termed “hotspots,” where the electromagnetic field intensity can be significantly enhanced. The enhanced electromagnetic fields within these hotspots result in a drastic increase in the Raman scattering cross-section of molecules adsorbed onto or near the metallic nanostructures. This phenomenon allows for the detection and characterization of analytes at extremely low concentrations, well below the detection limits achievable by conventional Raman spectroscopy. Furthermore, the amplification of Raman signals in SERS is not solely attributed to surface roughening but also critically depends on the plasmonic properties of the metal nanostructures and the resulting electric field enhancements. The combination of surface morphology (roughness) and the plasmonic response of the metallic nanostructures collectively contributes to the overall enhancement factor observed in SERS measurements.

* Corresponding author.
E-mail address: almasrim@missouri.edu (M. Almasri).

https://doi.org/10.1016/j.sbsr.2024.100686
Received 22 April 2024; Received in revised form 31 August 2024; Accepted 16 September 2024
Available online 24 September 2024

Over the past decades, several fabrication techniques have emerged to develop SERS sensors on flat substrates or fiber tips, aiming to achieve higher Raman signal enhancement. This is typically accomplished by roughening the sensing surface using methods such as chemical synthesis [10–12], photolithography [13], nanoimprint lithography [14], or nanosphere lithography [15–17]. For instance, chemical synthesis involves the use of metal nanoparticles (NPs) like gold (Au) to roughen the surface and amplify the signal by several orders of magnitude [18]. However, the random distribution of these NPs can result in uncontrollable hotspots, which eliminate the chances of maximizing Raman signal [19]. Photolithography utilizing equipment like electron beam lithography and focused ion beam can yield uniform and reproducible patterns [20]. However, they are cost prohibitive for production sensors, limiting their applications [21]. Nano-imprint lithography faces challenges, particularly in achieving precise alignment when patterning nanoscale molds in confined areas like fiber tips [22] Additionally, this method typically involves complex equipment, making it less cost-effective compared to alternative methods. Polystyrene nanosphere lithography is utilized as an alternative technique, where polystyrene nanospheres serve as a template to create, e.g., nano-islands [17,23]. However, controlling the pattern size remains a challenge in this approach. The Raman signal was enhanced using optical fibers of various shapes and types, such as fiber tip [24], hollow photonic crystal fiber (PCF) [25], and D-shaped fiber [26]. For example, hollow fiber increases the sample volume that interacts with light and NPs such [27]. However, applying the sample into the air holes in the PCF is challenging.

This manuscript discusses the development of a fiber-optic SERS sensor, with arrays of nanoantenna fabricated on a side of the fiber core. Highly ordered and periodic nanoantenna arrays were patterned using MPL. The sensor performance was studied as a function of disk diameter and sensing surface area using Rhodamine 6G (R6G) dye with concentrations ranging from 10^{-5} to 10^{-9} M.

2. Materials and methods

2.1. Biosensor design

To design the fibreoptics-based Surface Enhanced Raman Spectroscopy (SERS) sensor, the nanoantenna (nano disks) arrays are patterned on a side-polished multimode optical fiber core with dimensions of 105 μm × 1.7 mm and 105 μm × 7 mm. The schematic of the SERS sensor is depicted in Fig. 1. Notably, this design significantly increases the sensor's surface area when compared to SERS sensors patterned on the fiber tip with a similar core diameter. The induced SERS signal from is directly proportional to the increased fiber length, that is sensing surface area, surpassing the signal strength achievable from the fiber tip. Consequently, the sensor achieves higher sensitivity, leading to a very low limit of detection (LOD).

The size of nanodisks and the spacing between them critically influence their Localized Surface Plasmon Resonance (LSPR) properties. Our current design is limited to nanodisks with diameters ranging from 502 nm to 800 nm and a fixed periodicity of 1 μm. This is aimed at maximizing the enhancement factor through empirical optimization. However, we acknowledge the importance of aligning the LSPR wavelength more closely with the excitation wavelength of 532 nm to achieve optimal SERS enhancement. The spacing between the nanodisks is limited by the size of the microsphere used during exposure, which is fixed to 1 μm, and the disk diameter. The larger the disk diameter the smaller the spacing between the disks. Further reduction of the sphere size can reduce the spacing but switching to a smaller microsphere require further optimization of the photolithography steps, sphere preparation, and self-assembly processes. Therefore, considering the trade-off, we used 1 μm microsphere which also produced a periodicity of 1 μm.

This innovation opens avenues for a wide array of practical applications in chemical, biological, and gas sensing. In this design, an optical fiber was integrated into a 3-dimensional (3D) printed plastic mold,

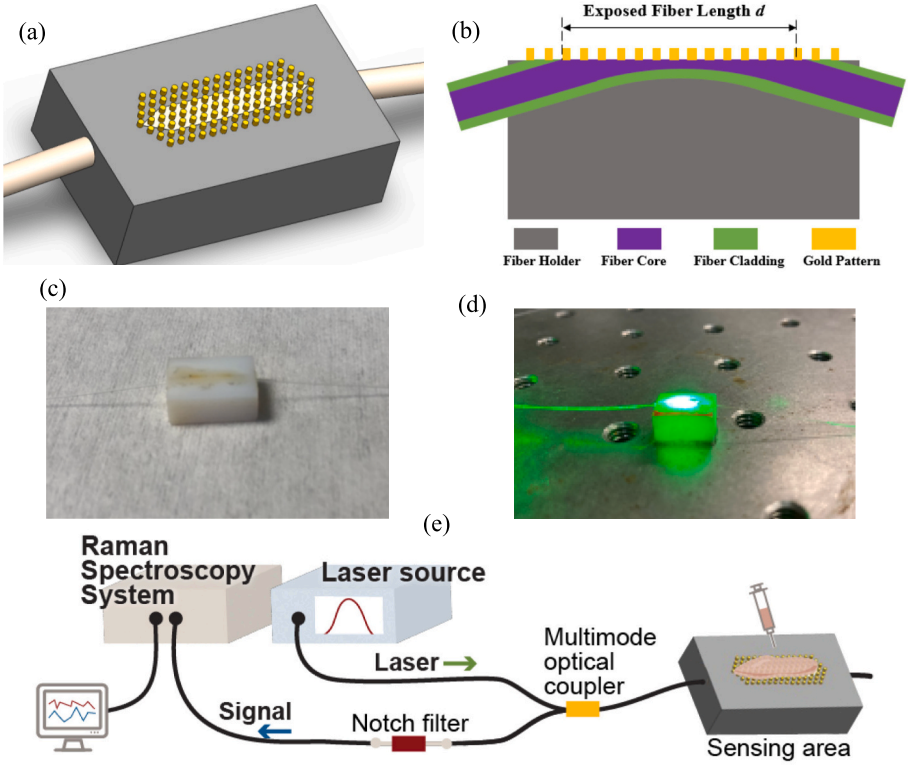

Fig. 1. (a) 3D view of the SERS sensor. The side-polished fiber fixed is inserted into the 3D printed plastic mold, (b) sideview of the nanoantenna arrays patterned on the side-polished multimode optical fiber, (c) printed 3D mold with the fiber inserted, (d) Experimental setup, (e) printed 3D mold with the sensor under testing.

facilitating polishing the fiber's cladding and a section of the core using alumina polishing sheets with a grain size of 0.5 mm. Operating on the principle of excitation with laser light at a wavelength of 532 nm (Laser-532-LAB-FC, Ocean Optics) and emission through a single fiber, the SERS sensor was designed to enhance sensitivity. To optimize the interaction with nanoantenna arrays and the analyte, the fiber was tilted at 15^{o} to increase the reflected light after scattering. The collected scattered light was directed to a Raman spectrometer (Enhanced QEPRO Raman, Ocean Optics) to produce SERS spectra. Nano disk arrays (that is nanoantenna arrays), composed of thin gold film, were patterned on the side-polished multimode optical fiber to roughen the surface area and amplify the SERS effects, enabling the acquisition of analyte spectra with high intensity even at low concentrations. The disk diameters were ranged from 502 nm to 800 nm, with a fixed periodicity of 1 μm.

Microsphere photolithography (MPL) was employed to create nanodisk arrays patterned on the side of the fiber. The sensor along with its cross-sectional side views are shown in Fig. 1.

To expose the cladding for the polishing process, the fiber's jacket in the middle portion (1.7 and 7.0 mm) was removed. A printing technology was employed to create the 3D plastic mold, facilitating the fixation of the fiber through the ports and aiding in the polishing process. The mold features a grooved trench measuring 1.7 and 7 mm in length at the top surface. This trench securely holds and exposes the fiber during the polishing process. Prior to inserting the fiber through the ports and securing it inside the trench, both the trench and the ports were filled with glue.

The SERS spectra, acquired from the reflected light after interacting with the analyte at the nanoantenna array's surface, serve to identify the molecular composition of the sample. These molecules possess specific vibrational modes that produce distinctive Raman spectral patterns. R6G, for instance, exhibits a vibrational fingerprint or SERS effect attributed to the scattering of light by the molecular vibrations of R6G. Subsequently, the detected R6G spectrum was compared with a reference R6G spectra, facilitating its identification and detection.

2.2. Fabrication

The SERS sensors were fabricated using microsphere photolithoraphy (MPL), creating periodic arryas of nanoantenna arrays on a side-polished multimode fiber with core. The diameter of the core and cladding diameters are 105 μm and 125 μm, respectively, and a length of approximately 10 cm. The fabrication process involved stripping the fiber's jacket in the middle portion with a length of 1.7 and 7 mm to expose the cladding for polishing. A plastic mold, created using 3D printing technology, with dimensions of 10 mm × 8 mm × 5 mm and grooved trenches of 1.7 mm and 7 mm in lengths, was used to hold the fiber firmly and aid the polishing process. The trench and ports were filled with glue, and the assembly was cured on a hotplate at 100 °C for 10 min. Afterward, the fiber, along with the mold, was manually polished using special fiber polishing papers with 5 μm and 1 μm gratings to ensure a smooth surface. Subsequently, Shipley 1805 photoresist was spun.

on the polished surface with a thickness of 400 nm, as shown in Fig. 2 (a), followed by the MPL process. A dry silica sphere of 1 μm diameter was mixed with butanol at a specific ratio. Using a pipette, a small drop of 4 μL of the mixture was dispensed onto the surface of a water-filled beaker confined by a rubber ring. The O-ring used for confining the monolayer colloidal crystal has a diameter of 2 in.. The ring needs to be big enough to cover the fiber assembly underneath the device. This size was chosen to provide a suitable confinement area while allowing for the formation of a stable monolayer colloidal crystal.

on the substrate. The silica microspheres with a diameter of $p = 1$ μm and a coefficient of variance of less than 3 % are dispersed in butanol to a concentration of 1 mg/mL with 5 mg of surfactant (Sodium lauryl sulfate). This concentration was selected based on previous studies to achieve a monolayer colloidal crystal formation with uniform packing density and particle arrangement. The ratio of silica microspheres to butanol was optimized to ensure proper suspension stability and controlled deposition during the experimental setup. Spheres will not form monolayer when the ratio is too high while spheres cannot form any layer when the ratio is too low. The capillary forces between the spheres, facilitated rapid self-assembly to form a close-packed lattice on the water surface. Subsequently, the water was slowly drained from the beaker, and eventually, the water surface came into contact with the submerged fiber and mold; thus, the microsphere layer was transferred to the polished fiber surface, as shown in Fig. 2(b). After successfully transferring the sphere layer, the fiber/mold was moved under a collimated UV illumination source ($\lambda = 365$ nm; 12 mW/cm^2 for intensity) and flood exposed for 1.5 s. Following exposure, the fiber/mold was submerged into a developer (MF 319) for 60 s and then washed with DI water. The sphere layer was removed during the development and washing step, as.

shown in Fig. 2(c). The patterned fiber/mold was subsequently placed inside an RF sputtering system for deposition of chromium (Cr) and gold (Au) with thicknesses of 5 nm and 60 nm, respectively, followed by a lift-off process, The lift-off process involves first patterning

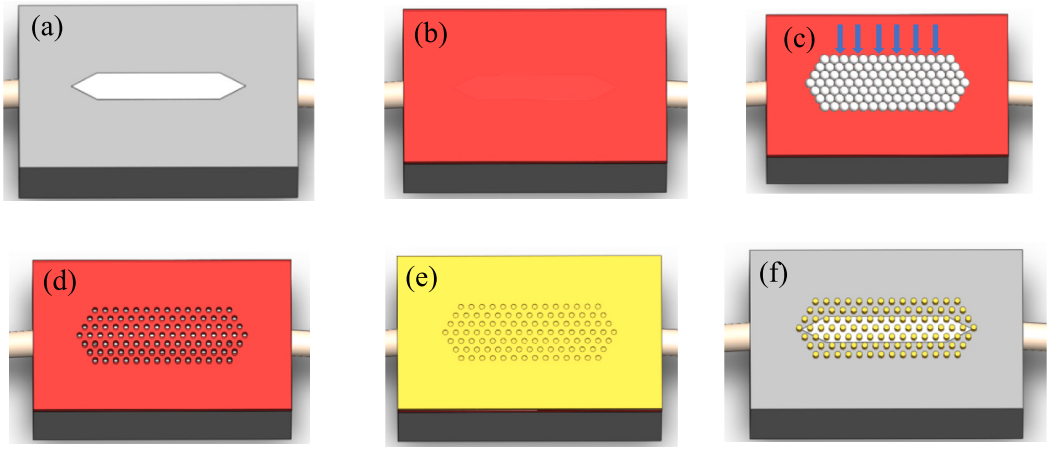

Fig. 2. Fabrication processing steps of the nanodisk arrays: (a) after fixing the fiber inside a 3D printed mold and polishing the fiber core from the side, (b) after spin coating the photoresist on a side-polished multimode optical fiber core, (c) after self-assembling the microspheres on the polished fiber surface, (d) after exposing the photoresist with UV light and creating nanoholes in the photoresist, the microsphere are removed during development, (c) after gold deposition, (f) after the gold layer was lifted off to create the nanodisk arrays. (For interpretation of the references to colour in this figure legend, the reader is referred to the web version of this article.)

the photoresist with nano holes on a side polished multimode optical fiber. This is followed by the deposition of gold (Au) layer with a thickness of 60 nm. The 60 nm thick Au layer adheres weakly to the photoresist layer. To break the sidewall of the Au layer, the device was placed inside acetone and the sonicator was turned on. This process broke the gold layer on the side edge and allowed acetone to dissolve the photoresist underneath the gold layer. Therefore, this allowed the gold to lift off in areas where the photoresist had been dissolved. This selective removal process is critical because it leaves behind the desired patterned structures—gold nanoantennas—on the polished fiber surface. In order to successfully lift of the metal, the photoresist needs to be 3 times thicker than the metal layer. Our resist thickness is 400 nm which is approximately 6 times thicker than the metal. Eventually, Au nanodisks with a diameter of 700 nm and a height of 60 nm were created on the surface of the fiber/mold, as depicted in Fig. 2(d). The diameter of the nanodisk pattern can be controlled by the amount of UV illumination, allowing for the creation of disks with various diameters. Scanning Electron Micrographs (SEMs) for the nanodisk pattern are shown in Fig. 3.

2.3. Experimental Setup

To validate the sensing capability of the SERS sensor, a Raman instrumental setup with a backscattered configuration was employed to measure the SERS signal, as shown in Fig. 1(c). The side-polished sensor was connected to a standard 1 × 2 coupler, allowing a 532 nm green laser to pass through. The light traveling within the fiber remained tightly confined in the core region until reaching the polished area where it interacts with the analytes and the nanoantenna arrays, thereby generating the scattered Raman signal. The Raman signal produced from the side-polished area was collected through the other end of the optical coupler, filtered through a notch filter, and directed into the QE Pro spectrometer. Raman signals were acquired using the OceanView software with a 500 ms integration time and 20-time averaging for each measurement. The Raman spectrum of R6G, a well-studied compound in the literature, served as a reference for subsequent data processing and analysis. For experimental purposes, five different concentrations of R6G ranging from 10^{-9} to 10^{-5} were prepared. During each experiment, a small drop of R6G was pipetted onto the exposed area, as shown in Fig. 1(c). The side surface of the SERS sensor underwent cleaning using DI water and compressed air after each measurement.

The multimode optical coupler used in our fiber-optic based SERS sensor is specifically designed by the manufacturer company (ThorLab, Model FG105LCA to efficiently transmit the excitation laser light at 532 nm and to collect the backscattered SERS signal. The key parameters and design considerations for the coupler includes the following. The coupler is optimized for broadband operation, effectively covering the wavelength range from 500 nm to 700 nm. This ensures low loss and efficient coupling for both the 532 nm excitation light and the broadband backscattered SERS signal. It is also designed to have minimal splicing loss with the side-polished sensor. The splicing process was carefully controlled to achieve a low insertion loss, typically around 0.2 dB. This low loss is crucial for maintaining the signal strength of both the excitation light and the backscattered Raman signal. Additionally, the coupling efficiency of the multimode coupler is optimized for the core diameter of 105 μm. The alignment and splicing process were refined to maximize the coupling efficiency, ensuring that the majority of the excitation light is directed towards the sensing region and the backscattered SERS signal is efficiently collected. The coupler design ensures strong and consistent coupling across a wide wavelength range. This broadband coupling capability is essential for accurately capturing the entire Raman spectrum, which spans from the Stokes shift to the anti-Stokes shift.

The side-polished multimode fiber is precisely aligned with the coupler to minimize any air gaps and misalignments that could lead to scattering losses. The polishing process was optimized to achieve a smooth and uniform surface, further enhancing the coupling efficiency. WThis design contributes significantly to the overall sensitivity and performance of our fiber-optic SERS sensor.

3. Results and discussion

To optimize the SERS sensor's configuration and determine the optimum sensitivity, two key factors were investigated: (1) the nano antenna's disk diameter at fixed periodicity. The disk diameter was manipulated by tuning the exposure dosage. The strength of the *E*-field is dependent on the size and shape of the disk array. The manipulation of nanodisk size through UV exposure is based on established principles of photolithography, where the duration and intensity of UV light directly influence the dimensions of patterned features. This technique has been widely documented in the literature and is routinely used in nanofabrication processes to control feature sizes. While we understand the importance of providing experimental validation, our manuscript focuses on the application of these fabricated nanodisks for Raman detection rather than on the detailed fabrication process itself. Our previous work discusses the details of creating disk diameters with various diameters on the fiber tip [28]. (2) the sensing surface area of the polished region. We hypothesized that increasing the surface area to some extent will maximize the S/N ratio and thus increase the sensitivity. Initially, the impact of the nanoantenna arrays were investigated by fabricating several sets of nanodisks with diameters ranging from 522 to 800 nm, a thickness of 60 nm on two sensing surface areas of 1.7 mm and 7 mm. Three disk diameters (522 nm, 602 nm, and 800 nm) were fabricated on a sensing area of 1.7 mm and tested with R6G dye at various concentrations ranging from 10^{-5} to 10^{-9} M. The resulting spectral peaks were plotted as a function of concentrations and as a function of diameters, as shown in Fig. 4. The obtained spectra revealed characteristic peak positions corresponding to R6G, which align well with the fingerprint Raman spectra of R6G found in the literature. The results demonstrates that the detection sensitivity is 10^{-9} M, as shown in Fig. 4(b). Furthermore, the results indicated that the SERS characteristic peak intensity increased with increasing disk diameter, as shown in

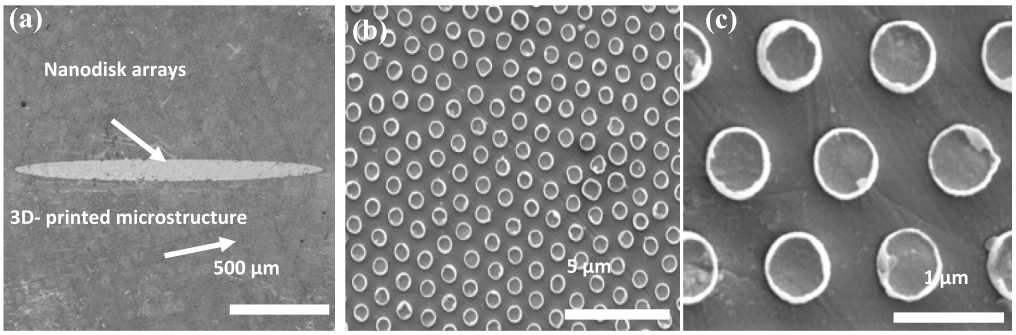

Fig. 3. SEMs of (a) a 3D printed mold with nanodisks arrays patterned, and (b and c) magnified views of the nanodisks arrays.

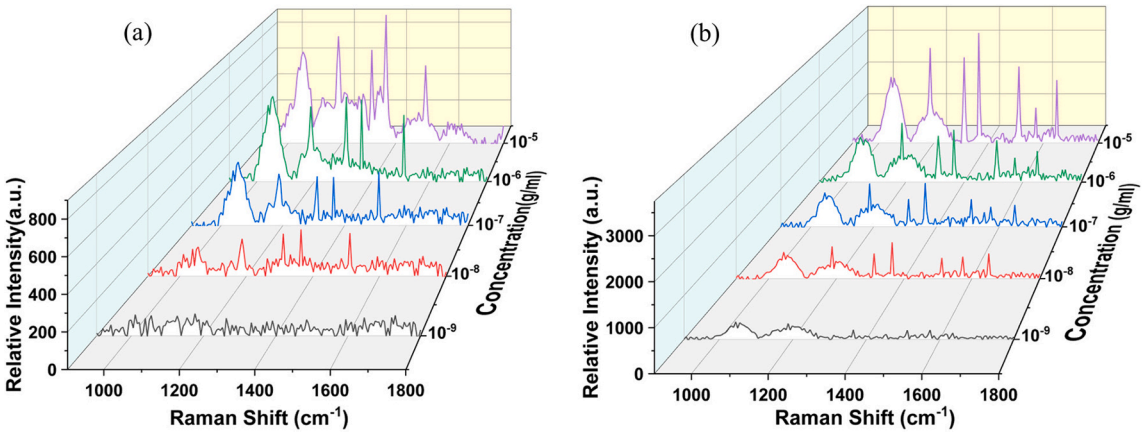

Fig. 4. Relative intensity versus concentration for SERS sensor with fixed disk diameters and sensing areas of (a) 602 nm and 105 μm ×1.7 mm, (b) 635 nm and 105 μm × 7 mm, respectively.

Fig. 5(a). All characteristic peaks of R6G, within the range of 800–1700 cm^{-1}, were detected with a notably higher signal. This result suggests that larger nanodisks diameter at fixed periodicity contribute to a relatively stronger SERS signal. The larger disk diameter reduces the spacing between the nanodisks, increasing the signal intensity. As a result, this enhancement significantly boosts Raman intensity compared to sensors with smaller nanodisks diameters. The current design sensitivity, i.e., limit of detection (LOD) was determined to be 10^{-9} M. However, the optimal disk diameter has not yet been determined. Future studies will focus on decreasing the spacing between the disks by reducing the periodicity, which may result in a much stronger *E*-field intensity between the disks, thereby enhancing the S/N ratio and potentially enabling the detection of R6G at even lower concentrations.

To assess the impact of the sensing surface area, the sensors were fabricated with two lengths of 1.7 mm and 7 mm with core diameter of 105 nm and with relatively similar disk diameters of 635 nm and 602 nm respectively. The sensors were tested with R6G dye at various concentrations and compared at a fixed concentration of 10^{-5} M, as shown in Fig. 5(b). Notably, the Raman intensity collected from the 7 mm sensing area sample exceeded that from the 1.7 mm sensing area sample, suggesting that a larger sensing area allows more photons to interact with the sample at the nanoantenna surface, reflecting some of the scattered light back towards the Raman system, resulting in a higher signal enhancement. The characteristic peaks of R6G were distinguishable even at a concentration as low as 10^{-9} M.

The observed increase in Raman intensity signal with larger sensing areas can be attributed to several factors related to the interaction between the light spot size, sensing surface, and analyte distribution. When the sensing area is increased, the interaction volume between the incident laser light and the analyte molecules is also increased. This larger interaction volume results in more effective scattering of light. The portion of the scattered light reflected back through the fiber and collected by Raman Instrument, thereby enhancing the Raman signal. The laser light spot size is typically constant for a given setup. However, with a larger sensing area, a greater number of analyte molecules within the illuminated region can contribute to the Raman scattering process. This results in an increase in the number of scattered photons being collected, thus improving the signal intensity. Additionally, with a larger sensing area, the probability of the laser interacting with more nanodisks also increases, which can further enhance the SERS effect due to the increased number of hotspots. Additionally, the diffusion of R6G sample on the sensing surface plays a crucial role in determining the uniformity and concentration of the analyte in contact with the nanodisks. On a larger sensing surface, the R6G sample can spread out more evenly, ensuring a more uniform distribution of the analyte molecules across the nanoantenna arrays. This uniform distribution can lead to more consistent and reliable enhancement of the Raman signal.

This study focused on analyzing the influence of nanoantenna disk diameter and sensing surface area on the performance of the SERS sensor. Future work will expand the number of samples and investigate additional parameters. For instance, we will examine the effect of reducing the periodicity on the SERS signal, where the periodicity is

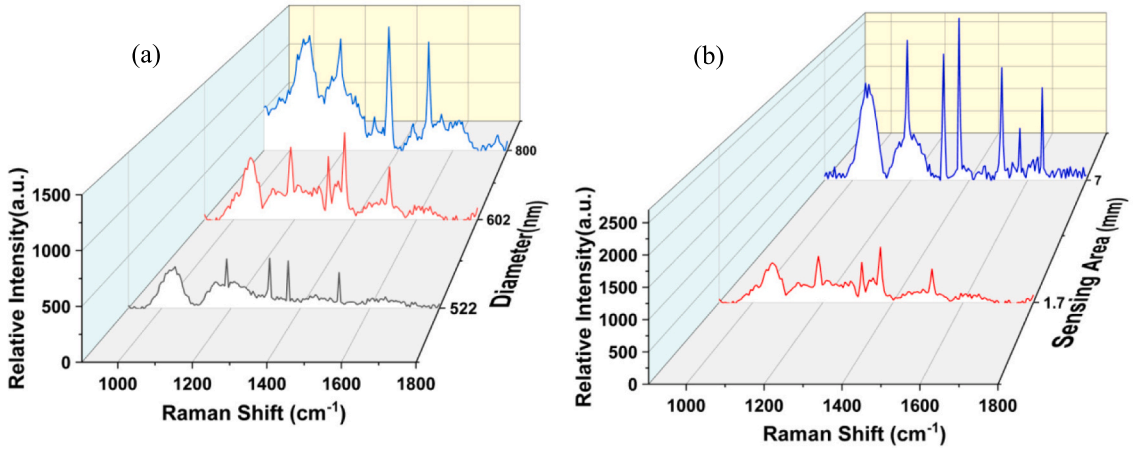

Fig. 5. SERS signal comparison between (a) disk diameters with a fixed area of 105 μm × 1.7 mm, and (b) sensing areas for relatively similar disk diameters (635 nm and 602 nm). The R6G concentration was 10–5 M.

determined by the size of the microsphere (with the periodicity equal to the microsphere's diameter). This study focused on a periodicity of 1 μm. Reducing it to sub-1 μm will require further optimization of microsphere preparation and self-assembly.

4. Conclusion

This work presents the design and fabrication fiber optics-based SERS sensor created on a side-polished multimode fiber. The fiber was integrated into a 3-dimensional (3D) printed plastic mold, facilitating polishing the fiber's core and cladding, and securing the fiber in place. This integration has enabled the creation of the nanoantenna arrays on the polished surface using low-cost Microsphere Photolithography (MPL) and lift-off processes. The fabrication of the nanoantenna on a side-polished multimode optical fiber is a new innovation. The sensor performance was evaluated using R6G dye with concentrations ranging from 10^{-5} to 10^{-9} M. The measured spectra exhibited characteristic peak positions corresponding to R6G, indicating successful detection. Notably, the sensor with the larger sensing surface area exhibited stronger signal intensities, directly proportional to the surface area. The characteristic peaks of R6G spectra were distinguishable even at lower concentrations. Moreover, the sensors with largest disk diameter at a fixed periodicity demonstrated the strongest signal, resulting in the highest sensitivity of 10^{-9} M. Future work will expand the number of samples and investigate additional parameters, periodicity for enhancing the performance and improve the sensitivity.

CRediT authorship contribution statement

Jiayu Liu: Conceptualization, Fabrication, Investigation, Testing, Analysis, Writing – original draft, Review and editing. **Bohong Zhang**: Testing, Software, Contribute to Writing – original draft. **Amjed Abdullah**: Fabrication, Investigation, Testing. **Sura A. Muhsin**: Fabrication, Review & editing. **Jie Huang**: Supervision, Resources. **Mahmoud Almasri**: Conceptualization, Methodology, Project administration, Resources, Supervision, Writing – original draft, Writing – review & editing.

Declaration of competing interest

We have no conflicts of interest to disclose.

Data availability

No data was used for the research described in the article.

Acknowledgements

Funding was provided in part by the University of Missouri internal funding.

References

[1] E. Le Ru, P. Etchegoin, Principles of Surface-Enhanced Raman Spectroscopy: And Related Plasmonic Effects, Elsevier, 2008.
[2] M. Reyes, M. Piotrowski, S.K. Ang, J. Chan, S. He, J.J. Chu, J.C. Kah, Exploiting the anti-aggregation of gold nanostars for rapid detection of hand, foot, and mouth disease causing enterovirus 71 using surface-enhanced Raman spectroscopy, Anal. Chem. 89 (10) (2017) 5373–5381.
[3] J.Y. Lim, J.S. Nam, S.E. Yang, H. Shin, Y.H. Jang, G.U. Bae, T. Kang, K.I. Lim, Y. Choi, Identification of newly emerging influenza viruses by surface-enhanced Raman spectroscopy, Anal. Chem. 87 (23) (2015) 11652–11659.
[4] Y.T. Yeh, K. Gulino, Y. Zhang, A. Sabestien, T.W. Chou, B. Zhou, Z. Lin, I. Albert, H. Lu, V. Swaminathan, E. Ghedin, A rapid and label-free platform for virus capture and identification from clinical samples, Proc. Natl. Acad. Sci. 117 (2) (2020) 895–901.
[5] P. Strobbia, Y. Ran, B.M. Crawford, V. Cupil-Garcia, R. Zentella, H.N. Wang, T. P. Sun, T. Vo-Dinh, Inverse molecular sentinel-integrated fiberoptic sensor for direct and in situ detection of miRNA targets, Anal. Chem. 91 (9) (2019) 6345–6352.
[6] A. Hakonen, P.O. Andersson, M.S. Schmidt, T. Rindzevicius, M. Käll, Explosive and chemical threat detection by surface-enhanced Raman scattering: a review, Anal. Chim. Acta 893 (2015) 1–3.
[7] S. Kumar, D.K. Lodhi, P. Goel, P. Mishra, J.P. Singh, A facile method for fabrication of buckled PDMS silver nanorod arrays as active 3D SERS cages for bacterial sensing, Chem. Commun. 51 (62) (2015) 12411–12414.
[8] S. Kumar, P. Goel, J.P. Singh, Flexible and robust SERS active substrates for conformal rapid detection of pesticide residues from fruits, Sensors Actuators B Chem. 31 (241) (2017) 577–583.
[9] Y. Li, L. Feng, J. Li, X. Li, J. Chen, L. Wang, D. Qi, X. Liu, G. Shi, Fabrication of an insect-like compound-eye SERS substrate with 3D ag nano-bowls and its application in optical sensor, Sensors Actuators B Chem. 330 (2021) 129357.
[10] Y.Q. Cao, K. Qin, L. Zhu, X. Qian, X.J. Zhang, D. Wu, A.D. Li, Atomic-layer-deposition assisted formation of wafer-scale double-layer metal nanoparticles with tunable nanogap for surface-enhanced Raman scattering, Sci. Rep. 7 (1) (2017) 5161.
[11] L. Li, S. Deng, H. Wang, R. Zhang, K. Zhu, Y. Lu, Z. Wang, S. Zong, Z. Wang, Y. Cui, A SERS fiber probe fabricated by layer-by-layer assembly of silver sphere nanoparticles and nanorods with a greatly enhanced sensitivity for remote sensing, Nanotechnology 30 (25) (2019) 255503.
[12] L. Tang, S. Li, F. Han, L. Liu, L. Xu, W. Ma, H. Kuang, A. Li, L. Wang, C. Xu, SERS-active au@ ag nanorod dimers for ultrasensitive dopamine detection, Biosens. Bioelectron. 71 (2015) 7–12.
[13] P. Zhang, S. Yang, L. Wang, J. Zhao, Z. Zhu, B. Liu, J. Zhong, X. Sun, Large-scale uniform au nanodisk arrays fabricated via x-ray interference lithography for reproducible and sensitive SERS substrate, Nanotechnology 25 (24) (2014) 245301.
[14] G. Kostovski, D.J. White, A. Mitchell, M.W. Austin, P.R. Stoddart, Nanoimprinted optical fibres: biotemplated nanostructures for SERS sensing, Biosens. Bioelectron. 24 (5) (2009) 1531–1535.
[15] K. Xu, R. Zhou, K. Takei, M. Hong, Toward flexible surface-enhanced Raman scattering (SERS) sensors for point-of-care diagnostics, Advanced Science. 6 (16) (2019) 1900925.
[16] S. Managò, G. Quero, G. Zito, G. Tullii, F. Galeotti, M. Pisco, A.C. De Luca, A. Cusano, Tailoring lab-on-fiber SERS optrodes towards biological targets of different sizes, Sensors Actuators B Chem. 339 (2021) 129321.
[17] M. Pisco, F. Galeotti, G. Quero, G. Grisci, A. Micco, L.V. Mercaldo, P.D. Veneri, A. Cutolo, A. Cusano, Nanosphere lithography for optical fiber tip nanoprobes, Light: Science & Applications. 6 (5) (2017) e16229.
[18] T.H. Chang, Y.C. Chang, C.M. Chen, K.W. Chuang, C.M. Chou, A facile method to directly deposit the large-scale ag nanoparticles on a silicon substrate for sensitive, uniform, reproducible and stable SERS substrate, J. Alloys Compd. 782 (2019) 887–892.
[19] S.Y. Ding, J. Yi, J.F. Li, B. Ren, D.Y. Wu, R. Panneerselvam, Z.Q. Tian, Nanomold-based plasmon-enhanced Raman spectroscopy for surface analysis of materials, Nat. Rev. Mater. 1 (6) (2016) 1–6.
[20] Q. Yu, S. Braswell, B. Christin, J. Xu, P.M. Wallace, H. Gong, D. Kaminsky, Surface-enhanced Raman scattering on gold quasi-3D nanostructure and 2D nanohole arrays, Nanotechnology 21 (35) (2010) 355301.
[21] I. Bruzas, W. Lum, Z. Gorunmez, L. Sagle, Advances in surface-enhanced Raman spectroscopy (SERS) substrates for lipid and protein characterization: sensing and beyond, Analyst 143 (17) (2018) 3990–4008.
[22] P. Jia, J. Yang, Integration of large-area metallic nanohole arrays with multimode optical fibers for surface plasmon resonance sensing, Appl. Phys. Lett. 102 (24) (2013).
[23] K. Xu, R. Zhou, K. Takei, M. Hong, Toward flexible surface-enhanced Raman scattering (SERS) sensors for point-of-care diagnostics, Adv. Sci. 6 (16) (2019) 1900925.
[24] T. Hutter, S.R. Elliott, S. Mahajan, Optical fibre-tip probes for SERS: numerical study for design considerations, Opt. Express 26 (12) (2018) 15539–15550.
[25] T. Gong, Y. Cui, D. Goh, K.K. Voon, P.P. Shum, G. Humbert, J.L. Auguste, X. Q. Dinh, K.T. Yong, M. Olivo, Highly sensitive SERS detection and quantification of sialic acid on single cell using photonic-crystal fiber with gold nanoparticles, Biosens. Bioelectron. 15 (64) (2015) 227–233.
[26] C. Zhang, A.M. Gu, Schwartzberg, J.Z. Zhang, Surface enhanced Raman scattering sensor based on D-shaped fiber, Appl. Phys. Lett. 87 (2005) 123105.
[27] F.M. Cox, A. Argyros, M.C. Large, S. Kalluri, Surface enhanced Raman scattering in a hollow core mold optical fiber, Opt. Express 15 (21) (2007) 13675–13681.
[28] I. Jasim, J. Liu, C. Zhu, M. Roman, J. Huang, E. Kinzel, M. Almasri, Microsphere photolithography patterned Nanohole Array on an optical Fiber, *IEEE*, Access 9 (2021) 32627–32633.

Jiayu Liu currently serves as a Process Integration Engineer at Coherent Corporation. He earned his PhD in Electrical Engineering and Computer Science from the University of Missouri, Columbia. His research interests include biosensors and microfluidics for food-borne pathogen detection, fiber-optic sensors, and microsphere photolithography.

Bohong Zhang received a Ph.D. degree in electrical engineering from the Missouri University of Science and Technology, Rolla, MO, USA, in 2022. He is currently an Assistant Research Professor with the Lightwave Technology Laboratory, Department of Electrical and Computer Engineering, Missouri University of Science and Technology, Rolla, MO, USA. His current research interests center around the advancement of optical and microwave sensors and instrumentation, focusing on their applications in intelligent infrastructures, biomedical sensing, and challenging environments. He has authored and co-authored over 30 journal and conferenced papers and filed four U.S. patents. Dr. Zhang is a

member of the Institute of Electrical and Electronics Engineers (IEEE), the Society of Photo-Optical Instrumentation Engineers (SPIE), the Optical Society of America (OSA), and the Association for Iron and Steel Technology (AIST) Organization. He has served as an invited reviewer to over 20 scientific journals and international conferences. He is also a Guest Editor in Electronics Journal.

Amjed Abdullah currently serves as a Semiconductor Process Engineer at TRUMF Corporation. He earned his PhD in Electrical Engineering and Computer Science from the University of Missouri, Columbia. His research interests include metasurface-based uncooled silicon germanium oxide (Si-Ge-O) infrared material and detectors, impedance-based microfluidic biosensors for rapid and accurate detection of foodborne pathogens, waterborne pathogens, viruses and proteins, optical fiber based plasmonic sensors and Surface-Enhanced Raman Scattering (SERS) sensors for chemical and biological sensing.

Sura A. Muhsin is a PhD student in Electrical Engineering and Computer Science at the University of Missouri (MU). Her research in impedance-based microfluidic MEMS biosensors for rapid and accurate detection of waterborne pathogens, viruses, and proteins, based uncooled silicon germanium oxide (Si-Ge-O) infrared material and detectors, and optical fiber-based plasmonic sensors and Surface-Enhanced Raman Scattering (SERS) sensors for chemical and biological sensing.

Jie Huang, pH.D. (Senior Member, IEEE), currently serves as the Roy A. Wilkens Endowed Associate Professor and Director of the Lightwave Technology Lab in the Department of Electrical and Computer Engineering at Missouri University of Science and Technology, Rolla, MO. With an extensive background in electrical engineering, Dr. Huang's research predominantly revolves around the innovative development of optical and microwave sensors, focusing on a diverse range of applications including energy systems, intelligent infrastructure, clean environments, biomedical sensing, and operation in harsh conditions. Over the past eight years at Missouri S&T, Dr. Huang has led and contributed to more than 30 externally-funded research projects, amassing a cumulative budget of approximately $36 M, with a personal shared credit of about $12 M. His projects have garnered support from esteemed organizations such as the National Science Foundation (NSF), National Institutes of Health (NIH), Army Research Office (ARO), Defense Advanced Research Projects Agency (DARPA), Air Force Office of Scientific Research (AFOSR), Department of Energy (DOE), and various National Laboratories, highlighting his prominence in the field of advanced sensor technologies. Dr. Huang's prolific academic output includes authoring or co-authoring over 150 refereed articles, alongside filing more than 10 U.S. patent applications. In recent years, his focus has shifted towards integrating fiber optic sensor technologies within the steelmaking industry. His notable achievements in this sector include the successful implementation of optical fiber sensors to monitor the chemical composition, temperature, and strain across the critical stages of an industrial-scale continuous casting machine. This implementation spans integral sections such as the electric arc furnace, tundish, nozzle, mold, and roller support, marking a significant advancement in the industry's technological capabilities.

Mahmoud Almasri is an Associate Professor of Electrical Engineering and Computer Science at the University of Missouri (MU). His laboratory investigates fiberoptics based Refractive Index sensors and Surface Enhanced Raman Spectroscopy (SERS) sensors, impedance based microfluidic biosensors, and metasurface integrated infrared material and uncooled detectors. His research is supported by NSF, ARO, ARL, USDA, MDC, LWI, and industry including B&V, and AOI.